Continuous Thermogravimetry under Cyclic Conditions

D. Monceau* and D. Poquillon*

Thermogravimetry during cyclic oxidation of metallic alloys is described. A methodology is given in order to determine the Net Mass Gain, the Gross Mass Gain, the total mass of spalled oxide, the rate of metal consumption and the average oxide scale thickness as a function of the number of cycles. The fraction of oxide scale which spalls at each cycle can be also calculated, and the parabolic constant can be estimated at each cycle. Two examples are given: the cyclic oxidation of a NiAl single crystal in flowing oxygen at 1150°C, and the cyclic oxidation of alloy P91 at 800°C in laboratory air. Advantages and disadvantages of this technique are discussed in regards to classical interrupted tests in crucibles. Thermogravimetry during cyclic oxidation appears to be a powerful tool in order to model and quantify the cyclic oxidation test which is of great interest in order to qualify the resistance of materials to oxidation in conditions close to their actual use, but a specific aspparatus need to be developed in order to obtain data in an efficient and economical manner. A new apparatus designed for this purpose is described briefly.

KEY WORDS: cyclic oxidation; thermogravimetry; high-temperature oxidation modeling; NiAl; P91.

INTRODUCTION

Metallic alloys are frequently subjected to combined environmental attack and mechanical stresses during their actual service life. Their resistance to this complex loading relies partly on their ability to form a protective oxide scale, i.e. an oxide layer with low growth kinetics and high adherence to the alloy. The nature and kinetics of the growth of the oxide layer is, most of the time, studied using isothermal laboratory tests. The quantitative testing of

*Cirimat UMR 5085 (INPT/UPS/CNRS), Ensiacet, 118 route de Narbonne, F-31077 Toulouse, Cedex 04, France.

adherence at high temperature is a difficult subject, and several methods have been developed including laser ultrasonics,[1,2] and the inverted-blister test.[3] Spalling cannot be directly deduced from oxide-scale adherence, because it also depends on the intensity of stresses (growth stresses and stresses due to thermal-expansion-coefficient mismatch), on the thickness and mechanical properties of the oxide scale and on the creep of the metallic substrate during cooling. Thermal-shock experiments or the evaluation of the critical temperature drop before spalling[4,5] are a more direct way to measure spalling. The fundamental measurements of oxidation kinetics, scale adherence, high-temperature growth stresses measurements by X-ray diffraction, combined with visco-plastic finite-element modeling of the substrate-oxide scale system should result in the qualification of the ability of the alloy to form a protective oxide scale. To do so, these measurements need to be performed as a function of time because the microstructure and chemistry of the alloy under the scale change with time, especially when the objective of long time-life prediction is pursued. Model developments are also necessary in order to relate these fundamental measurements to the actual protectiveness of oxide scales on metallic parts under their actual conditions of use. Consequently, when testing the resistance to oxidation of high-temperature materials, the cyclic-oxidation test[6] is used as a reference because it integrates isothermal-oxidation kinetics, oxide-scale adherence, mechanical stresses, metallic alloy and oxide creep and the evolution of these properties with time, for conditions close to the actual conditions of use.

To fill the gap between the measurements of physical data (oxidation kinetics, interfacial energy, growth stresses, coefficients of thermal expansion, mechanical properties of the alloy and of the oxide,...) and the cyclic-oxidation test, comprehensive scientific work is necessary.[7,8] But on the other hand, technological development and understanding of the cyclic-oxidation test also needs to be done.

Because the cyclic-oxidation test combines the effects of oxidation kinetics, mechanical stresses, adherence and microstructural evolution, it is often recognized as complex and used as a qualitative or "screening-test" tool. Improvements in lifetime predictions could be obtained through the quantification of cyclic-oxidation-test results. For that purpose, two routes are followed: (1) modeling of the kinetics,[9–11] (2) development of new instruments or measurement methods. This paper deals with the second point, and specifically with the use of continuous thermogravimetry for cyclic conditions.

BACKGROUND

Most of the available cyclic-oxidation gravimetric data have been obtained by discontinuous experiments.[12,13] Samples are periodically removed

from the furnace to be weighed and then replaced in the furnace. To obtain reproducible cooling and heating rates, dwell times at high and at low temperature, an automatic cyclic-oxidation test is preferred.[14] Nevertheless, weighing of the samples is generally done manually. Two choices can be made. Samples can be hung in the furnace atmosphere or they can be placed in open or closed crucibles. In the first case (no crucible), only the Net Weight Gain is measured, i.e. the variation of the mass of the sample with its remaining attached oxide scale. In the second case (with crucible), both the Net Mass Gain and the Gross Mass Gain (variation of the mass of the crucible with the sample and with spalled oxide scale inside) is measured. None of these two solutions is fully satisfying. Indeed, if only the Net Mass Gain is measured, it is not possible to dissociate the mass gain due to oxygen uptake and the mass loss due to oxide spalling.[13,15] In the second case many experimental problems arise: (1) it is impossible to obtain rapid heating and cooling when samples are inside crucibles, (2) it is difficult to ensure that specimen experience a constant gas composition and gas velocity, (3) the variation of the crucible mass itself may decrease the precision of the measurement, (4) some spalls of oxide may escape from an opened container. With both experimental procedures, the specimen handling is difficult (spalling, contamination) and time consuming (expensive). Moreover, the transfer of the samples out of the atmosphere studied can affect the results, especially because of ambient humidity. Furthermore, sample transfers affect the dwell time and the temperature of the low-temperature dwell.

Previous uses of Continuous Thermogravimetry for Cyclic Conditions

Few authors have reported the use of high-resolution continuous thermogravimetry for cyclic conditions. Early works from Lacombe's group[16,17] report the use of a Cahn balance to compare the mass gains of FeNiCrAl and FeNiCrAlY alloys during cyclic oxidation (20 hr dwell at 1200°C or 1300°C followed by 4 hr cooling to 250°C). This nice experiment clearly demonstrates the beneficial effect of yttrium on alumina-scale growth kinetics and spalling. In,[18] thermogravimetry has been used to qualitatively compare oxidation kinetics under isothermal and cyclic oxidation, for single-crystal, nickel-base, superalloys. Thanks to this technique, the extent of damage due to cycling can be clearly identified as well as the moment when extensive damage during cyclic condition begins. Krupp *et al.*[19] have also used thermogravimetry to help the modeling of internal-corrosion processes. Comparing experimental NMG records with COSP's NMG simulation, the moment when a certain amount of oxide has spalled is determined and used as a starting point in the finite-difference calculation of inward oxygen and nitrogen diffusion in the metallic matrix and subsequent internal oxidation

and nitridation. In another work, Vangeli *et al.*[20,21] have used thermogravimetry in cyclic conditions as a test of adherence of oxides on austenic steels. A critical weight gain for which significant spallation occurs was determined. Indeed, on time–mass plots in the 1000–1200°C range, it was possible to observe qualitatively a critical NMG over which the extent of spalling at each cooling becomes large.

In these previous works, the use of continuous thermogravimetry in cyclic conditions has solved some of the experimental problems reported before for cyclic-oxidation testing with manual weighing. Nevertheless, it is a quite expensive method if one utilizes a classic thermobalance during hundreds or thousands of hours for a single sample. Moreover, only the Net Mass Gain was measured when using TGA. Finally, some specific equipment needs to be developed to ensure high heating (10 to 100°C/s) and cooling rates without taking the samples out of the thermobalance's furnace atmosphere. In fact, most of the disadvantages of the continuous-mass measurement during cycling can be eliminated using a careful analysis of the gravimetric curves (see below) and thanks to the development of a new kind of thermobalance.[22]

EXPERIMENTAL PROCEDURE

The experimental part of the work presented here concerns the cyclic oxidation of an alumina-forming intermetallic alloy with low oxidation kinetics (single-crystal beta-NiAl), and a steel with relatively high oxidation kinetics at 800°C (P91 alloy).

Sample Purity and Initial Surface Preparation

Disk samples (nom. 8 mm diameter × 1 mm thickness) were cut by electroerosion from single-crystal NiAl fabricated at ONERA. Disk specimens with (100) oriented surfaces were mechanically polished up to a "mirror" finish using a $\frac{1}{4}$-μm diamond paste. The samples were ultrasonically cleaned in ethanol and acetone, and dried. The P91 sample was of rectangular shape ($20 \times 10 \times 1$ mm) polished to 1200 grit, ultrasonically cleaned in ethanol and acetone, and dried. Compositions of the alloys are given in Table I.

Thermogravimetry

Two thermogravimetric apparati were used. NiAl samples were oxidized in a commercial Setaram TAG24s thermobalance. This apparatus has the advantage of combining a good accuracy with a limitation of buoyancy effects due to a symmetrical furnace arrangement. Drawbacks of this apparatus to perform cyclic-oxidation testing are: (1) it is expensive, (2) it tests

Table I. Composition of the NiAl Single Crystal and P91 Alloy

wt.%	Fe	Cr	Ni	Mo	Mn	Si	C	P
NiAl	0.014		73			0.033	0.004	0.0002
P91	89	8.6	0.26	0.93	0.41	0.36	0.10	0.013

wt.%	S	Al	V	Nb	N	Mg	B
NiAl	0.003	27			0.0005	0.007	0.0002
P91	0.003	0.01	0.205	0.070	0.053		

only one sample at a time and (3) it has a modest heating rate (90°C/min) and slow cooling (about 30 min from 1200°C to 100°C). To avoid these problems, a new kind of thermogravimetric apparatus was developed. This apparatus combines a six halogen-lamps-furnace with 6 independent alumina sample holders and 6 balances. We report here, one test of this apparatus, for one P91 sample oxidized at 800°C with 5 minute high-temperature dwells. This test was first of all dedicated to thermal performances, and was not realized with a high precision balance. The use of the lamp furnace allows fast heating and cooling as described later.

Characterization of the Morphology and Microstructure of the Oxide Scale

The oxidation of single-crystal NiAl is part of a larger study using SEM and XRD, which is presented in another publication.[23]

CONTINUOUS THERMOGRAVIMETRY MEASUREMENTS

Characteristic values for the cyclic-oxidation test can be calculated easily from the continuous recording of the mass.[24] These include the Net and Gross Mass Gains, the mass of spalled oxide, the average thickness of the adherent oxide scale, the rate of metal consumption and the oxide-growth kinetics (see Table II and Fig. 1).

Because of the buoyancy effect and of possible convection currents, the apparent mass of the sample depends on the temperature and may change during fast heating and cooling. For this reason, we focus on the measurement of mass only during the high-temperature dwell times. Indeed, buoyancy effects on the apparent mass measurement are compensated during cooling and heating, and convection currents are transient phenomena during rapid change of temperature. A continuous recording of the apparent mass with an inert sample (e.g. alumina) allows determination if the mass is constant during one high-temperature dwell and if it does not change from one dwell to another. Once this has been checked out, it is possible to experimentally access both the Net Mass Gain (NMG) and the Gross Mass Gain (GMG) by recording only two characteristic points in each cycle: the

Table II. Calculation of Oxide-Growth Kinetics and Spalling Using the Continuous-Mass Measurement During Cyclic Oxidation

Description of the quantity	Units	
Oxygen/metal mass ratio in the oxide (alumina Al_2O_3) (where M_O and M_{Al} are the molar mass of oxygen and aluminum)	No u.	$r = 3M_O/(3M_O + 2M_{Al})$
Density of oxygen in the oxide (where V_o is the molar volume of oxygen in the oxide in cm^3/mol)	g/cm^3	$\rho_O = M_O/V_O$
Density of the oxide	g/cm^3	$\rho = \rho_O/r$
Measured mass gain per unit area at the beginning of the high-temperature dwell n	mg/cm^2	M_n^{bg}
Measured mass gain per unit area at the end of the high-temperature dwell n	mg/cm^2	M_n^{end}
Mass gain per unit area during the high-temperature dwell n	mg/cm^2	$\Delta M_n = (M_n^{end} - M_n^{bg})$
Net Mass Gain per unit area at the end of n cycles, neglecting oxidation during heating and cooling	mg/cm^2	$NMG_n = M_{n+1}^{bg}$
Mass of spalled oxide between cycle n and cycle $n + 1$, per unit area of sample surface (negative value if spalling occurs)	mg/cm^2	$SOX_n = (M_{n+1}^{bg} - M_n^{end})$
Gross Mass Gain per unit area at the end of n cycles, neglecting oxidation during heating and cooling	mg/cm^2	$GMG_n = \sum_{j=1}^{n} (M_j^{end} - M_j^{bg})$
Mass of metal loss at the end of n cycles	mg/cm^2	$MET_n = \frac{2M_{Al}}{3M_O} GMG_n$
Cumulated mass of spalled oxide at the end of n cycles, per unit area of sample surface	mg/cm^2	$TOX_n = \sum_{j=1}^{n} (M_{j+1}^{bg} - M_j^{end})$
Mass of adherent oxide after n cycles, per unit area	mg/cm^2	$AOX_n = M_{n+1}^{bg} + \left(\frac{1}{r} - 1\right) \sum_{j=1}^{n} (M_j^{end} - M_j^{bg}) - M_1^{bg}$
Average thickness of the oxide scale after n cycles	cm	$e_n = \frac{AOX_n}{\rho}$
Proportion of the mass of the adherent oxide which spalled at cycle n. This term equals the sample surface fraction that spalled if spalling occurs at metal/oxide interface (and if the spalling does not depend on oxide thickness)	n.u.	$P_n = \frac{SOX_n}{AOX_n}$
Parabolic constant during high-temperature dwell i (overestimated—see text)	$mg^2/cm^4/s$	$k_{pn} = 2rAOX_n \left(\frac{M_n^{end} - M_n^{bg}}{\Delta t}\right)$
Parabolic constant during high-temperature dwell i (overestimated—see text), from the local fitting of a parabola (necessitate to have at least 3 mass gain data during the high temperature dwell)	$mg^2/cm^4/s$	$k_{pn} = \frac{1}{C}$ where $t = A + Bm + Cm^2$

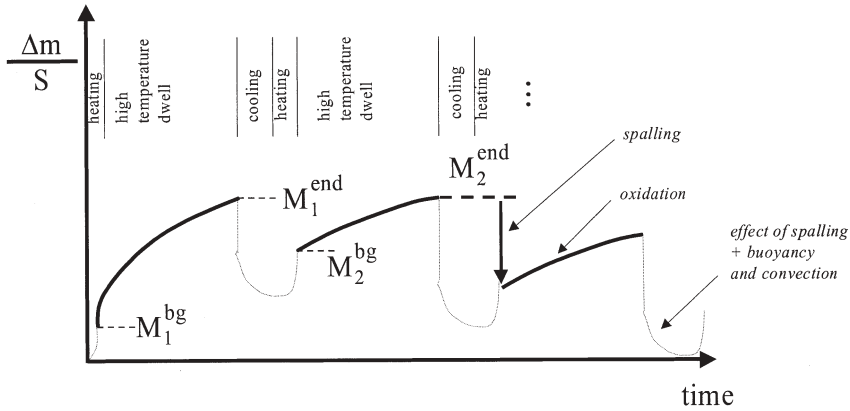

Fig. 1. Schematics of an expected mass variation during cyclic oxidation of metals, with mass increase due to oxidation at high temperature and mass loss during cooling due to spalling. Mass variation at constant high temperature is recorded by continuous thermogravimetry. Mass changes during heating and cooling are not used for quantification because of the effects of convection and buoyancy.

Net Mass Gain at the beginning of the high-temperature dwell n (M_n^{bg}) and the Net Mass Gain at the end of the high-temperature dwell n (M_n^{end}).

Measurement of the Net Mass Gain (NMG)

The series of M_n^{bg} points is equivalent to a "classic" NMG manual recording during discontinuous measurements. The mass gain due to oxidation (ΔM_n) during the high-temperature dwell is easily calculated as $\Delta M_n = (M_n^{end} - M_n^{bg})$ (see Table II).

Measurement of the Mass of the Spalled OXide (SOX)

Assuming that spalling occurs during cooling or low-temperature dwell and/or during heating, and that most of the oxide growth occurs during the high-temperature dwell, it is then possible to calculate the mass of the spalled oxide (SOX_n) at the end of cycle n as the difference $SOX_n = M_{n+1}^{bg} - M_n^{end}$ (Table II). By summation, it is then possible to plot the total mass of spalled oxide per unit area of sample surface (TOX_n) as a function of the Gross Mass Gain, as suggested by Newton *et al.*[25] in order to determine a possible critical-oxide thickness for time of life modeling.[26]

Measurement of the Gross Mass Gain (GMG)

From the calculation of the mass of spalled oxide at each cycle, it is now obvious to determine the GMG at the end of cycle n (GMG_n), as

shown in Table II:

$$GMG_n = \sum_{j=1}^{n} (M_j^{\text{end}} - M_j^{\text{bg}}) \tag{1}$$

This equation neglects the mass gain due to oxidation during the first heating. Indeed, for low oxidation kinetics (less than 100 μg mass gain in 1 hr), it is difficult to dissociate mass gain due to oxidation and buoyancy effect during heating. For larger oxidation kinetics, one would have to correct this equation by adding the mass gain during the first heating. The total mass of consumed metal per unit area of sample surface (MET_n) is then given by:

$$MET_n = \frac{2M_{\text{Al}}}{3M_{\text{O}}} GMG_n \tag{2}$$

Calculation of the Adherent Oxide Thickness

In order to model the phenomenon of oxide growth and of subsequent spalling, it is of great interest to calculate the *average* thickness of the scale which remains attached to the sample (e_n). This can be done through the determination of the mass of the adherent oxide scale per unit area of sample surface (AOX_n):

$$AOX_n = M_{n+1}^{\text{bg}} + \left(\frac{1}{r} - 1\right) \sum_{j=1}^{n} (M_j^{\text{end}} - M_j^{\text{bg}}) - M_1^{\text{bg}} \tag{3}$$

and

$$e_n = \frac{AOX_n}{\rho} \tag{4}$$

where ρ is the density of the oxide. This determination of the average oxide-scale thickness is useful in order to compare the calculated oxide thickness with the experimental one as determined by SEM, and to formulate and discuss models linking the oxide-scale thickness with the extent of spallation. Nevertheless, one should remember that some oxide may have spalled but still be attached to the sample, and that the value of the oxide thickness is an average between spalled and unspalled surface areas.

Calculation of the Isothermal-Oxidation Kinetics (k_P)

Because the average oxide-scale thickness is known at each cycle, the isothermal-oxidation kinetics can be determined. In the case of parabolic growth kinetics during the high-temperature dwell, two ways of calculating the parabolic rate constant are given in Table II. First, assuming a simple parabolic law:

$$k_P = 2m\frac{dm}{dt} = 2r^2 AOX_n \frac{dAOX_n}{dt} \approx 2rAOX_n \frac{M_n^{\text{end}} - M_n^{\text{bg}}}{\Delta t} \tag{5}$$

because "m" is the mass gain per unit area (mg/cm^2) corresponding to the protective adherent oxide layer, and where r is the ratio of oxygen to metal mass in the oxide, and Δt is the duration (s) of the high-temperature dwell.

The second way to calculate the parabolic rate constant during the high-temperature dwell "n" consists of fitting a parabola to the Net Mass Gain curve:

$$t = a + bm + cm^2$$

where

$$k_P = \frac{1}{c} \tag{6}$$

It was shown previously that this fitting can be used locally, even after a transient stage of different kinetics.[27] The same approach is valid in this case, even if the thickness of the oxide scale is not known at the beginning of the high-temperature dwell because of successive spalling. This last calculation procedure implies experimental determination of a mass-gain curve for each high-temperature dwell.

Nevertheless, an oxide scale after successive localized spalling events is not expected to have a uniform thickness. The calculated value of the parabolic constant k_P when the protective oxide-scale thickness is not uniform is over-estimated.[28] This error was estimated using a numerical simulation (Monte Carlo model[29] similar to the numerical COSP code[10]). Simulated NMG curves are computed with a typical value of k_P for alumina-formers at 1100°C ($k_P = 10^{-6}$ mg^2/cm^4/s), with a high-temperature dwell time of $\Delta t = 3600$ s and with several values of the spalling probability "p" taken as constant, and assuming that spalling occurs at the metal/oxide interface (this last assumption maximizes the error made by assuming a uniform oxide-scale thickness). Table III reports the errors made by using Eq. 5 to calculate the k_P at cycle n. These errors are negligible when the proportion of the surface area which spalls at each cycle is low (below 1%), but one should be careful because this error increases with the number of cycles because of accumulated errors. For comparison, fitted values (ranging in the [0.04%–10%] interval) of "p" using the simple p-k_P model have been provided by Poquillon & Monceau.[11]

Table III. Errors Produced Using Eq 5 to Calculate the Parabolic Constant from the Cyclic-Oxidation NMG Curve

Error: $\frac{k_P(\text{calc}) - 10^{-6}}{10^{-6}}$	$p = 10\%$	$p = 1\%$	$p = 0.1\%$	$p = 0.01\%$
At $n = 10$ cycles	+ 28%	+ 4%	+ 1%	+ 0.0%
At $n = 1000$ cycles	+ 49%	+ 45%	+ 31%	+ 4%

Such a direct measurement of k_P from cyclic-oxidation data is impossible using discontinuous-mass measurements.

Detection of Oxide-Scale Damage

The continuous recording of mass also allows determination of the precise moment when some oxide detaches from its substrate as was previously shown by Evans and Lobb[4] for Ni–Cr alloys or Bouhanek *et al.*[30] for Ni-base superalloys. In these works, high-sensitivity thermogravimetry is used to grow an oxide scale of known and controlled thickness before following the mass during cooling in order to determine a critical temperature drop when the first spall is detected.[31] Moreover, the continuous recording during the high-temperature dwell allows determination if some spalling or scale rupture with subsequent increase of oxidation kinetics occurs at high temperature. Then, the continuous mass recording during cyclic oxidation is a detection tool of oxide damage, and could be correlated with acoustic emission.

Modeling of Cyclic-Oxidation Kinetics

Models of cyclic-oxidation kinetics use two constitutive laws: a kinetic description of the isothermal oxidation during the high-temperature dwell (usually parabolic or sub parabolic kinetics) and a description of spalling (occurrence and extent). The spalling extent is generally given as the proportion of the surface area where oxide scale spalls after cycle n (P_n). In the simplest models, P_n is either a constant,[9,11] or a Heavyside function of a critical value of the oxide scale thickness.[32–34] In numerical models, it is possible to include a more-complex dependence of P_n over the scale thickness, for example a polynomial law.[10,35] It is also possible to simulate the effect of oxide fracture inside the oxide scale, because spalling does not always occur at the metal/oxide interface.

To compare these models and experimental data, continuous thermogravimetry is a tool of interest, because it allows the measurement of P_n as a function of the number of cycles and of time but also as a function of the average oxide-scale thickness whose calculation has been described previously. The same can be done with the parabolic constant k_P which can also be calculated at each cycle. It is very useful to access independently to P_n and k_P in a single experiment in order to quantify the cyclic-oxidation test and to develop its modeling. The evaluation of P_n and k_P at each cycle permits detection of the occurrence of breakaway oxidation, and even slight changes in the nature of the oxide formed. This is also of particular interest in the case of alloys which undergo a large amount of transient oxidation before a steady-state scale is developed (e.g. single-crystal Ni-base superalloys).

For the same purpose of time of life modeling, Nicholls *et al.*[26] recommend recording and plotting the mass of spalled oxide as a function of the Gross Mass Gain,[25] using samples in crucibles. The continuous thermogravimetry is an automatic and alternative way to perform these measurements without experiencing the experimental difficulties reported in the Background paragraph.

RESULTS AND DISCUSSION

In the following, two examples of continuous-mass recording during cyclic oxidation are reported and analyzed.

Cyclic Oxidation of Single-Crystal NiAl

A NiAl single crystal was oxidized in a SETARAM TAG24s thermobalance. The experiment consisted of 168 cycles including dwell times of 45 min at 1150°C and 30 min dwell times at 150°C. Heating was at a constant rate of 60°C/min and cooling was controlled at 20°/min down to 150°C. The experiment was conduced in flowing oxygen. The obtained Net Mass Gain recording, without any data processing, is given in Fig. 2. This curve includes 12,000 data points. The general "classic" shape of cyclic-oxidation data combining mass gain due to oxidation and mass loss due to spalling is obtained, without any apparent occurrence of breakaway after

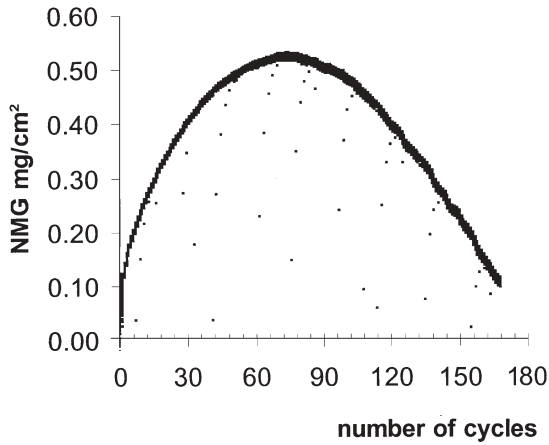

Fig. 2. Experimental Net Mass Gain of a NiAl single crystal (100) oxidized during 168 cycles of 45 min at 1150°C in flowing oxygen. Data set contains 12,000 points recorded with a SETARAM TAG24s thermobalance.

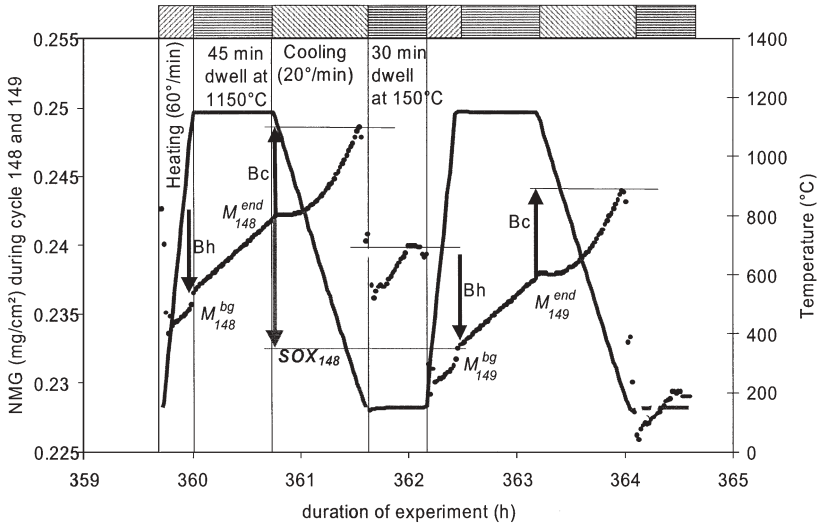

Fig. 3. Enlargement of Fig. 2 with superimposition of the recorded temperature during 2 cycles. Definition of the mass gain due to oxidation ($\Delta M_{148} = (M^{end}_{148} - M^{bg}_{148})$), mass of spalled oxide ($SOX_{148} = (M^{bg}_{149} - M^{end}_{148})$), buoyancy effect during heating (*Bh*) and cooling (*Bc*).

$168 \times 0.75 = 126$ hr at 1150°C. This last observation was confirmed by X-ray diffraction which detected only alpha alumina in the oxide scale.

On Fig. 2, some data points recorded during heating and cooling, are seen to lie outside the general shape of the NMG curve. The recorded signal is detailed in Fig. 3 which is an enlargement of Fig. 2 during two cycles (148th and 149th) selected at random for illustration. On this enlargement, it is seen that the mass gain during the high-temperature dwell is about 10 μg at 1150°C. This value justifies the use of a high-precision microbalance for alumina formers, if one wants to follow oxidation at each cycle. During cooling, an apparent mass gain is recorded ("*Bc*" on Fig. 3), whose intensity compensates the apparent mass loss during heating ("*Bh*"). These mass changes can be attributed to the buoyancy effect linked to the change of temperature and to the difference between the oxidizing sample and the alumina counter-sample (both samples are inside symmetrical furnaces in SETARAM TAG24s). In 1 atm oxygen, the apparent variation of mass *Bc* due to buoyancy during cooling from 1150°C to 150°C is given by:

$$Bc = -\frac{MP\Delta V}{R}\left(\frac{1}{423} - \frac{1}{1423}\right) \tag{7}$$

where ΔV is the difference between the volume of the oxidizing sample minus the volume of the counter-sample, P the total pressure, R the gas constant, and M, the molar mass of the gas. In 1 atm oxygen, one gets:

$$Bc = -0.64\Delta V \qquad (\mu g/mm^3) \tag{8}$$

In Fig. 3, it can be seen that Bc is about 10 μg, which is consitent with a volume difference of about 16 mm^3 between samples (i.e. 30% of the volume of the sample). During the low-temperature dwell at 150°C, the apparent mass is constant after a transient stage. The mass difference between the end of the high-temperature dwell and the low-temperature dwell is the sum of the buoyancy effect and of spalling during cooling. Because spalling may also occur during the low-temperature dwell,[23] or during heating, and because the buoyancy effects during heating and cooling compensate each other, the spalling at the end of the 148th cycle is measured as the difference $SOX_{148} = M_{149}^{bg} - M_{148}^{end}$. This calculation is done with the assumption that oxidation during cooling and heating is negligible relative to spalling and mass gain during the high-temperature dwell. This assumption may generate errors which may accumulate with the number of cycles. For example, on Figs. 4–6, the spalling fraction P and the experimental Total mass of spalled OXide (TOX) are negative during the first cycles, because the extent of spalling is low and the sample still oxidizes during the beginning of cooling and the end of heating (the average oxide thickness is low). From the data of Fig. 2, the parabolic constant k_P can be calculated for each cycle, using Eq. 5 or the local fitting of a parabola (Eq. 6). These results are reported in Table IV and compared with known values for the same material oxidized under isothermal conditions. After analysis, it appears that the calculated k_P from Eq. 6 should be taken only as estimated values, because for NiAl the mass gain during the 45 minute dwell at 1150°C is only about 5 to 10 μg. The mass-gain curve is apparently linear during high-temperature dwell and calculation of k_P from the curvature of this curve is subject to a large uncertainty. Additional experiments are in progress with longer dwells, higher temperature, and using alloys with higher oxidation kinetics, in order to precisely determine the errors made during these calculations. Nevertheless,

Table IV. Calculated Parabolic Constants at Each Cycle During Cyclic Oxidation of Single Crystal NiAl (100) at 1150°C in Flowing Oxygen

	N = 2	N = 20	N = 48	N = 90	N = 150	k_P (18 hr isothermal oxidation in flowing O_2)
k_P (Eq. 5) 10^{-7} $mg^2/cm^4/s$	+15	+19	+23	+23	+24	+8.0
k_P (Eq. 6) 10^{-7} $mg^2/cm^4/s$	+5.2	+2.9	+1.3	+2.9	+4.1	

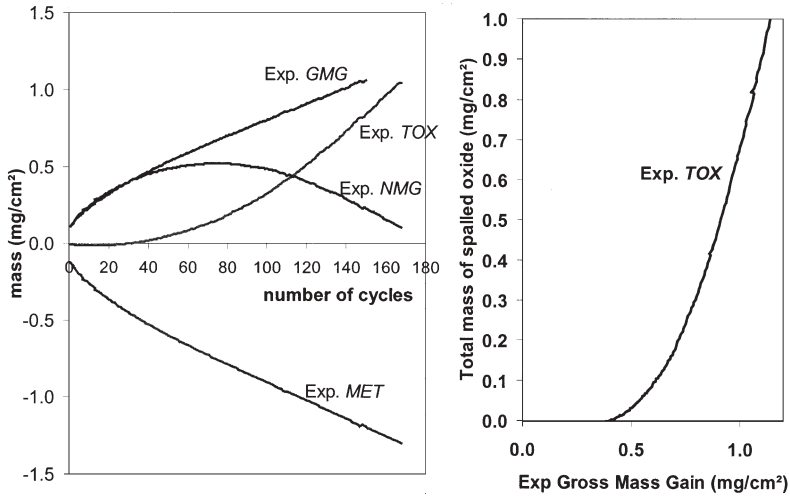

Fig. 4. Experimental Net Mass Gain (NMG) (Fig. 2) and deduced Gross Mass Gain (GMG), mass of METal consumption (MET), Total mass of spalled OXide (TOX), using thermogravimetry during thermal cycling (NiAl, 168×45 min dwells at 1150°C in O_2).

these mass gains of 5 to 10 μg could be measured during this experiment, and this allows determination if oxidation kinetics remain controlled by a protective alpha-alumina layer. Indeed, at 1150°C, parabolic constants higher than 10^{-5} mg^2/cm^4/s are expected for transition aluminas or spinel $NiAl_2O_4$, and about $3 \cdot 10^{-3}$ mg^2/cm^4/s for NiO.

From the recording of the Net Mass Gain M_i^{bg} and M_i^{end} data points, GMG, MET and TOX can be calculated (see text and Table II). The resulting values are plotted on Fig. 4 as a function of the number of cycles. These experimental data are useful to test and develop cyclic-oxidation models. For example, the TOX vs. GMG plot can be drawn on Fig. 4 (right side), as recommended by Newton *et al.*[25] in order to determine if a critical thickness can be identified and to evaluate its value.

The average oxide-scale thickness and proportion of the oxide mass which spalls at each cycle can be calculated as explained previously. These data are plotted in Fig. 5 as a function of the number of cycles. It can be seen that the average oxide-scale thickness increases up to about 3.4 μm after 110 cycles, then remains approximately constant. The proportion of oxide which spalls at each cycle also increases smoothly and seems also to reach a constant value after 110 cycles. Then, two regimes are identified. During the first regime (1 to 110 cycles), the Net Mass Gain curve goes to a maximum value (75th cycle) and then decreases with a linear asymptotic behavior. This linear

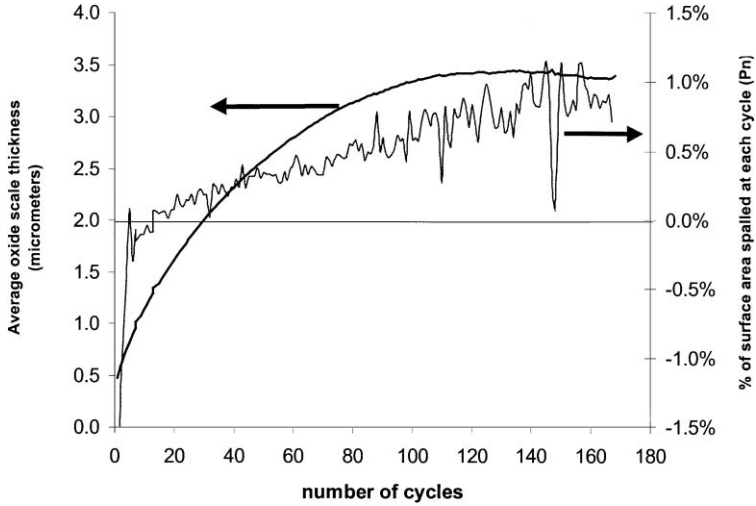

Fig. 5. Average oxide-scale thickness and fraction of the adherent oxide which spalls at each cycle, calculated from the continuous recording of sample mass during thermal cycling (see text) (NiAl, 168×45 min dwells at 1150°C in O_2).

decrease of NMG (after about 110 cycles) constitutes the second regime and corresponds to a constant, average oxide-scale thickness. This observation is consistent with the analytic or numerical simulations of the Smialek 78's model, Poquillon & Monceau's simple statistical model "pk_P" and COSP. Moreover, the continuous-thermogravimetric analysis during thermal cycling allows determination that the fraction of adherent oxide which spalls at each cycle (P_n) increases during the first regime, most probably with the increasing oxide-scale thickness. Plotting P_n as a function of the average oxide-scale thickness (Fig. 6) shows that P_n is a linear or polynomial function of the average oxide-scale thickness during the first regime, from about 1 μm (corresponding to the mass gain after the first high-temperature dwells) to about 3.5 μm. During the second regime, the oxide-scale thickness is constant, and P_n takes random values around an average of about 0.8%, as it can be seen in Fig. 5. If the experiment was conducted for several hundreds of cycles, most of the "life" of the sample would be around this fixed point ($P_n = 0.8\%$, $e = 3.5$ μm), as long as no breakaway occurs. This plot should not be interpreted as the occurrence of a critical thickness of 3.5 μm, because the present experimental data do not show a drastic increase of P_n at a given value of oxide thickness. The constant thickness value is just the consequence of the stationary state of the second regime, when the mass of spalled oxide at each cycle equals the mass of the newly-formed oxide during the previous

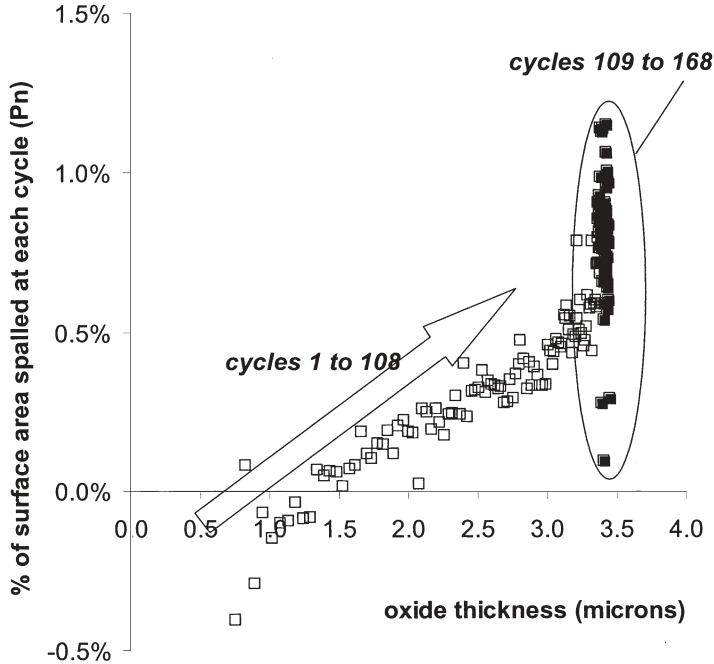

Fig. 6. Fraction of the adherent oxide which spalls at each cycle as a function of the average oxide-scale thickness deduced from the continuous recording of sample mass during thermal cycling (see text) (NiAl, 168×45 min dwells at 1150°C in O_2).

high-temperature dwell. These thermogravimetric data allow fitting a function P_n as a function of the average oxide-scale thickness.

Cyclic Oxidation of P91

A P91 steel sample was oxidized in the new apparatus briefly described previously. The experiment consisted of 13 cycles including dwell times of 5 min at 800°C and 5 min cooling to 140°C. Heating was regulated at a constant rate of 600°C/min, and cooling was regulated at 600°C/min during the first part of the cooling (see Fig. 7). At maximum furnace power (6×1000 W halogen lamps), other tests have shown a maximum heating rate of 5400°C/min up to 1200°C and cooling rate of 1800°C/min at 1100°C on a 150 μm-thick specimen (alloy 718). The obtained Net Mass Gain recording without any data processing is given in Fig. 8. For this experiment, a 10-μg-sensitivity balance (Sartorius) was used. Work is in progress to include SETARAM 1-μg-precision (0.1 μg sensitivity) balances in the apparatus,

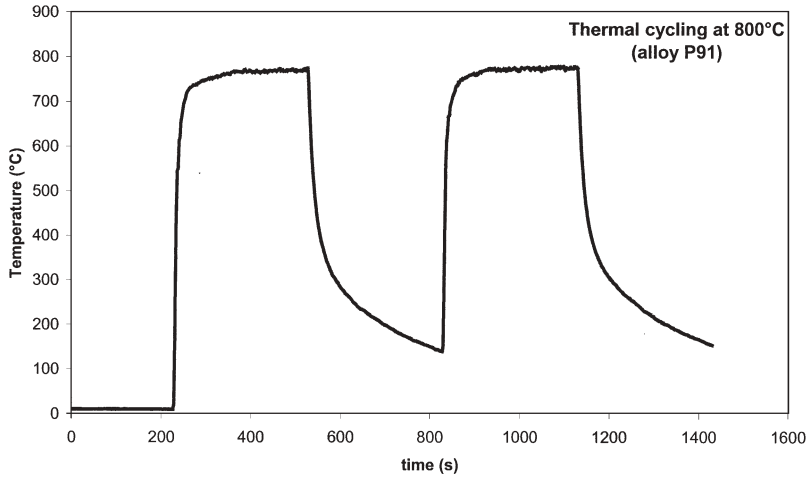

Fig. 7. First two thermal cycles of sample P91 ($20 \times 10 \times 1$ mm). High heating and cooling rates are obtained with a specifically designed thermobalance combining microbalances and a lamp furnace of 6×1000 W allowing the simultaneous cyclic oxidation of 6 samples under controlled atmosphere (see text).

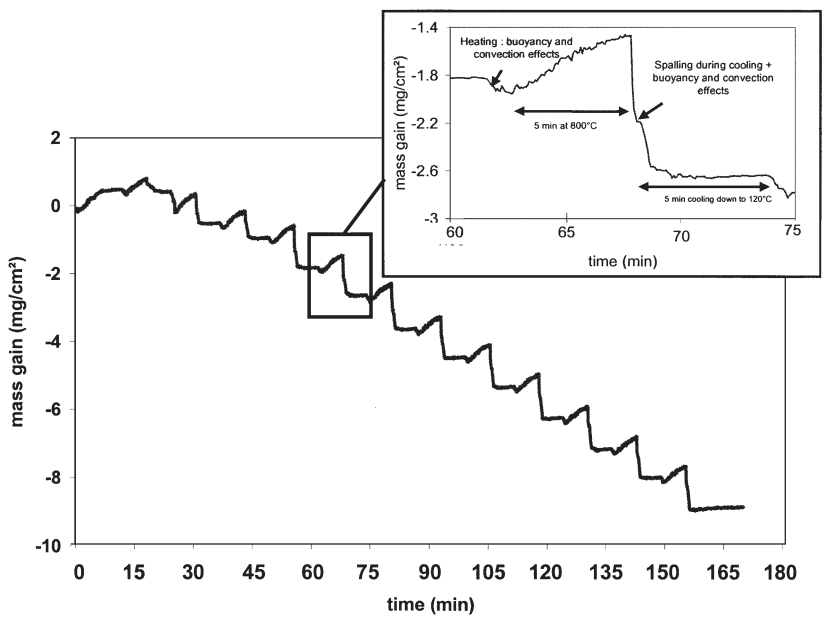

Fig. 8. Experimental Net Mass Gain of a P91 alloy oxidized during 13 cycles of 5 min at 800°C in laboratory air. These data are obtained with a specifically designed thermobalance (see text).

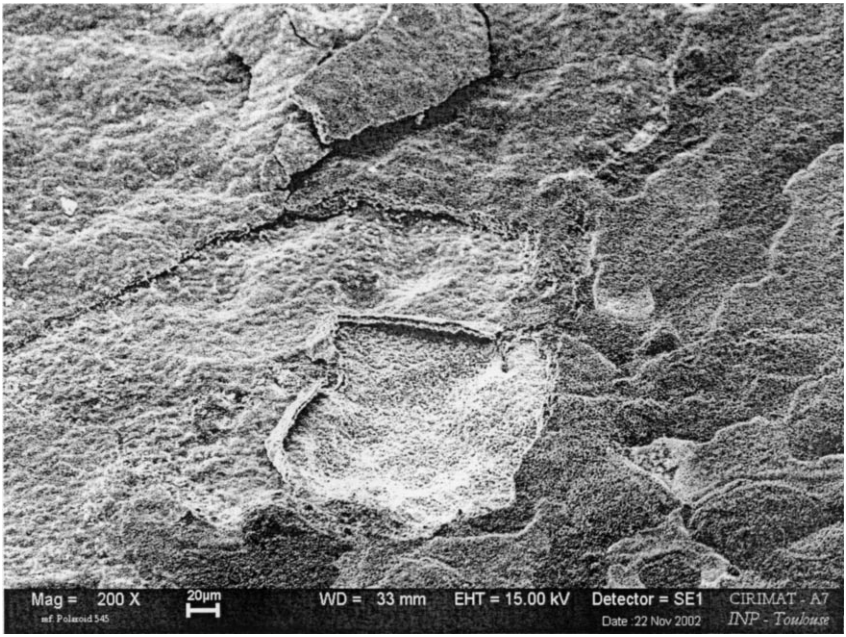

Fig. 9. Scanning-electron-microscope view (tilted 60°) of the oxidized surface of P91 sample after 13 cycles at 800°C in air.

in order to be able to follow alumina-formers, cyclic-oxidation kinetics. Because this apparatus does not make use of a counter sample to compensate for buoyancy, this effect was estimated to be $Bc = -346\left(\frac{1}{413} - \frac{1}{1073}\right) 200 = -103\,\mu g$, i.e. $-23\,\mu g/cm^2$ during cooling which is small compared to the 0.4 to 0.5 mg/cm^2 mass gain during one high-temperature dwell.

As for the previously-reported experiment on the NiAl single crystal, the NMG curve for P91 shows a "classic" general shape with a mass increase during its first part, followed by a mass loss and eventually a stationary regime with a global linear mass loss. Mass gain data could also be obtained during each high-temperature dwell, and the spalling extent at each cycle evaluated between these high-temperature dwells. The microstructural observation of this oxidized-steel sample after 13 cycles at 800°C in air, shows that the analysis is more complicated than for the NiAl sample. Difficulties arise from the fact that some of the spalled or fissured-oxide scale remains attached to the sample (Fig. 9). As a consequence, the calculation of the fraction of the adherent oxide which spalls at each cycle, and the calculation of the average adherent oxide-scale thickness are dubious. Therefore, Eq. 5 should not be used to calculate the k_P at each cycle, but the local fitting of a

parabola (Eq. 6) should be preferred because the corresponding isothermal-kinetics model allows for a mass of non-protective oxide.[27]

It can be seen on this sample that the spalling does not occur at the metal/oxide interface, but inside the oxide-scale which is multi-layered. Then, one should be careful when trying to model the kinetics of cyclic oxidation.

CONCLUSIONS

The continuous recording of mass during cyclic oxidation is a powerful means to obtain cyclic-oxidation kinetics data. Using the data analysis described in the present paper, this technique allows determination of not only the Net Mass Gain (NMG) evolution, but also the Gross Mass Gain (GMG), the Total mass of spalled OXide (TOX), the mass of Metal loss (MET) the average oxide-scale thickness (e), the parabolic rate constant (k_P) and the fraction (P_n) of adherent oxide which spalls at each cycle. Analysis of the experimental correlations between these functions is useful to model the kinetics of cyclic oxidation. For example, the analysis of the cyclic oxidation of a beta-NiAl single crystal has allowed us to determine the evolution of the fraction of spalled oxide P_n as a function of the average oxide-scale thickness, and to discuss the concept of a critical-oxide-scale thickness. Such modeling is necessary for the prediction of time of life of components exposed at high temperature in oxidizing atmosphere.

Continuous thermogravimetry advantageously replaces discontinuous-measurement experiments during which samples need to be placed in crucibles in order to measure independently the Net Mass Gain and the mass of spalled oxide. Indeed the crucibles used are a source of experimental difficulties. Moreover, several mass measurements during each cycle are necessary to dissociate the mass gain due to oxidation and the mass loss due to spalling. Both measurements are important in order to qualify the material's resistance to cyclic oxidation in terms of resistance to spalling and low oxidation kinetics, as it was presented on a two-dimensional performance chart.[11,36]

The main disadvantages of this technique are, first, it is expensive, because most high-temperature-materials, cyclic-oxidation studies require many samples during very long experiments (1000 to 20000 hr); second, it allows only low heating and cooling rate when classic thermobalances are used for this application. That is why a specific apparatus needs to be developed, which should allow several samples to be analyzed at the same time and will have an economical gain linked to the small amount of experimental work needed to run an experiment. The fast-cycling thermobalance briefly described here will be presented in more detail in another publication.[22]

ACKNOWLEDGMENTS

The authors would like to thanks J. C. Salabura for the conception and building of the new cyclic-oxidation apparatus, P. Josso and M.-P. Bacos (ONERA-Chatillon-F) for the elaboration of NiAl single crystal, B. Viguier for single-crystal orientation and scientific discussion on NiAl oxidation, C. Levade from INSA Toulouse and D. Caillard from CEMES for providing respectively Laue diffraction and spark-machinig facilities, Djar Oquab for helping in SEM observations and for discussing some of the present results, Laeticia Des for sample preparation. This study was partly funded by the French Research Ministry grant ''ACI 2000 Surfaces and Interfaces'' (AdheronS! project).

REFERENCES

1. G. Rosa, M.-H. Nadal, and R. Oltra, *Journal of Applied Physics* **91**, 6744 (2002).
2. G. Rosa, P. Psyllaki, R. Oltra, S. Costil, and C. Coddet, *Ultrasonics* **39**, 355 (2001).
3. J. Mougin, M. Dupeux, A. Galerie, and L. Antoni, *Materials Science and Technology* **18**, 1217 (2002).
4. H. E. Evans, and R. C. Lobb, *Corrosion Science* **24**, 209 (1984).
5. K. Bouhanek, D. Oquab, and B. Pieraggi, *Materials Science Forum* **251–254**, 33 (1997).
6. M. Schütze, and W. J. Quaddakkers, eds., *The European Federation of Corrosion*, 1999.
7. H. E. Evans, *Materials at High Temperatures* **12**, 219 (1994).
8. M. Schütze, *Oxidation of Metals* **44**, 29–61 (1995).
9. J. L. Smialek, *Metallurgical and Materials Transactions A* **9A**, 309 (1978).
10. C. E. Lowell, C. A. Barrett, R. W. Palmer, J. V. Auping, and H. B. Probst, *Oxidation of Metals* **36**, 81 (1991).
11. D. Poquillon, and D. Monceau, *Oxidation of Metals* **59**, 409 (2003).
12. H. J. Grabke, and D. B. Meadowcroft, eds., *The European Federation of Corrosion*, 1995.
13. J. R. Nicholls, and M. J. Bennett, in *Cyclic oxidation of high temperature materials*, M. Schütze, and W. J. Quadakkers, eds. (IOM Communications Ltd, London, 1999), Vol. EFC 27, p. 437.
14. J. Smialek, J. A. Nesbitt, C. A. Barrett, and C. E. Lowell, in *Cyclic oxidation of high temperature materials*, M. Schütze, and W. J. Quadakkers, eds. (IOM Communications Ltd, London, 1999), Vol. EFC 27, p. 148.
15. B. A. Pint, P. F. Tortorelli, and I. G. Wright, in *Cyclic oxidation of high temperature materials*, M. Schütze, and W. J. Quadakkers, eds. (IOM Communications Ltd, London, 1999), Vol. EFC 27, p. 111.
16. P. Moulin, *PhD thesis* (Paris Sud, Orsay, 1978), p. 91.
17. J. C. Pivin, D. Delaunay, C. Roques-Carmes, A. M. Huntz, and P. Lacombe, *Corrosion Science* **20**, 351 (1980).
18. S. Y. Chang, U. Krupp, and H. J. Christ, in *Cyclic oxidation of high temperature materials*, M. Schütze, and W. J. Quadakkers, eds. (IOM Communications Ltd, London, 1999), Vol. EFC 27, p. 63.
19. U. Krupp, S. Y. Chang, A. Schimke, and H. J. Christ, in *Lifetime modelling of high temperature corrosion processes*, M. Schütze, W. J. Quadakkers, and J. R. Nicholls, eds. (Maney Publishing, London, 2001), Vol. EFC 34, p. 148.
20. P. Vangeli, and B. Ivarsson, *Materials Science Forum* **369–372**, 785 (2001).
21. P. Vangeli, in *Cyclic oxidation of high temperature materials*, M. Schütze, and W. J. Quadakkers, eds. (IOM Communications Ltd, London, 1999), Vol. EFC 27, p. 198.
22. J.-C. Salabura, and D. Monceau, *Materials Science Forum*, paper accepted (2004).

23. D. Poquillon, D. Oquab, B. Viguier, F. Senocq, and D. Monceau, *Materials Science and Engineering A*, submitted (2003).
24. D. Monceau, communication at COTEST meeting, Madrid, February (2003).
25. R. Newton, M. J. Bennet, J. P. Wilber, J. R. Nicholls, D. Naumenko, W. J. Quadakkers, H. Al-Badairy, G. J. Tatlock, G. Strehl, G. Borchardt, A. Kolb-Telieps, B. Jonsson, A. Westerlund, V. Guttmann, M. Maier, and P. Beaven, in *Lifetime modelling of high temperature corrosion processes*, M. Schütze, W. J. Quadakkers, and J. R. Nicholls, eds. (Maney publishing, Franckfurt, 2001), Vol. European Federation of Corrosion Publications 34, p. 15.
26. J. R. Nicholls, R. Newton, M. J. Bennet, H. E. Evans, H. Al-Badairy, G. J. Tatlock, D. Naumenko, W. J. Quadakkers, G. Strehl, and G. Borchardt, in *Lifetime Modelling of High Temperature Corrosion Processes*, M. Schütze, W. J. Quadakkers, and J. R. Nicholls, eds. (Maney publishing, Franckfurt, 2001), Vol. European Federation of Corrosion Publications 34, p. 83.
27. D. Monceau, and B. Pieraggi, *Oxidation of Metals* **50**, 477 (1998).
28. H. Coradin, R. Peraldi, J. Lacaze, and D. Monceau, poster at ''Jeunes chercheurs'', Montpellier (1998).
29. D. Monceau, communication in *Journées d'Automne de la Société Française de Métallurgie et de Matériaux SF2M* (Paris, 2000).
30. K. Bouhanek, D. Oquab, and B. Pieraggi, *High Temperature Corrosion and Protection of Materials, Materials Science Forum* **251–254**, 33 (1997).
31. H. E. Evans, *International materials reviews* **40**, 1 (1995).
32. W. J. Quadakkers, and K. Bongartz, *Mater. Corros.* **45**, 232 (1994).
33. I. Gurupa, S. Weinbruch, D. Naumenko, and W. J. Quadakkers, *Mater. Corros.* **51**, 224 (2000).
34. J. R. Nicholls, R. Newton, M. J. Bennett, H. E. Evans, H. Al-Badairy, G. J. Tatlock, D. Naumenko, W. J. Quadakkers, G. Strehl, and G. Borchardt, in *Lifetime modelling of high temperature corrosion processes*, M. Schütze, W. J. Quadakkers, and J. R. Nicholls, eds. (Maney Publishing, London, 2001), Vol. EFC 34, p. 83.
35. J. S. Smialek, and J. V. Auping, *Oxidation of Metals* **57**, 559 (2002).
36. D. Poquillon, and D. Monceau, in *TMS Annual Meeting*, Peter K. Liaw, Raymond A. Buchanan, Dwaine L. Klarstrom, Robert P. Wei, D. Gary Harlow, and Peter F. Tortorelli, eds. (TMS, San Diego, 2003), Vol. Materials Lifetime Science Engineering, p. 165.